

Quantum Similarity Testing with Convolutional Neural Networks

Ya-Dong Wu,¹ Yan Zhu,^{1,*} Ge Bai,² Yuexuan Wang,^{3,4} and Giulio Chiribella^{1,5,6,†}

¹*QICI Quantum Information and Computation Initiative, Department of Computer Science, The University of Hong Kong, Pokfulam Road, Hong Kong*

²*Centre for Quantum Technologies, National University of Singapore, Block S15, 3 Science Drive 2, 117543, Singapore*

³*AI Technology Lab, Department of Computer Science, The University of Hong Kong, Pokfulam Road, Hong Kong*

⁴*College of Computer Science and Technology, Zhejiang University, Zhejiang Province, China*

⁵*Department of Computer Science, Parks Road, Oxford, OX1 3QD, United Kingdom*

⁶*Perimeter Institute for Theoretical Physics, Waterloo, Ontario N2L 2Y5, Canada*

The task of testing whether two uncharacterized quantum devices behave in the same way is crucial for benchmarking near-term quantum computers and quantum simulators, but has so far remained open for continuous-variable quantum systems. In this Letter, we develop a machine learning algorithm for comparing unknown continuous variable states using limited and noisy data. The algorithm works on non-Gaussian quantum states for which similarity testing could not be achieved with previous techniques. Our approach is based on a convolutional neural network that assesses the similarity of quantum states based on a lower-dimensional state representation built from measurement data. The network can be trained offline with classically simulated data from a fiducial set of states sharing structural similarities with the states to be tested, or with experimental data generated by measurements on the fiducial states, or with a combination of simulated and experimental data. We test the performance of the model on noisy cat states and states generated by arbitrary selective number-dependent phase gates. Our network can also be applied to the problem of comparing continuous variable states across different experimental platforms, with different sets of achievable measurements, and to the problem of experimentally testing whether two states are equivalent up to Gaussian unitary transformations.

Introduction. Comparing unknown quantum states based on experimental data [1–4] is crucial for benchmarking quantum simulations and near-term quantum computers [5]. A natural approach in this context is to choose a trusted device as a reference standard, and to compare other devices to it. For example, the trusted device could be built and maintained by a quantum computing company, while the other devices could be owned by users in distant laboratories. One way to compare two unknown quantum devices is to estimate their overlap [1, 6–11], which is also useful for tasks like quantum state discrimination and classification [12–15]. Recently, Elben *et al.* proposed an approach named cross-platform verification [1], which uses only local Pauli measurements to experimentally estimate the overlap between two multiqubit states. This approach has been recently demonstrated on quantum systems with more than ten qubits [16].

An alternative approach to characterize quantum states from measurement data is provided by deep neural networks [17–26], which can work with a smaller amount of data when the states under consideration belong to state families with sufficient structure, such as the family of ground states of the Ising model with different values of the couplings and of the magnetic field. Recently, neural networks for testing the similarity of quantum states

have been developed for the tasks of state discrimination and classification [27–32]. The existing methods, however, generally assume that the state of the system is identifiable by a finite set of predetermined labels. For the purpose of comparison of uncharacterized quantum states, this assumption is too restrictive, as it prevents the application to continuous families of quantum states, such as the families of coherent states and cat states in quantum optics.

In this Letter, we develop a convolutional neural network for testing the similarity of quantum states drawn from a continuously-parametrized state family. For sufficiently regular families, our network manages to tell different states apart using noisy and incomplete measurement data, without requiring randomization over an exponentially large set of measurements, or correlations between measurements performed on different states. The network is trained with data from a fiducial set of quantum states sharing structural similarities with the states to be compared. After training, the network embeds the measurement data into a low-dimensional feature space in a way that reflects the similarity of quantum states. This low-dimensional state representation is then used by the network to decide whether the two given states are the same or not. Our approach is inspired by a classical technique for the recognition of human faces in blurred and incomplete images [33], a task that shares similarities with the task of comparing continuous-variable quantum states from finite-statistics approximations of their Wigner function.

We test the performance of our network on noisy cat

* yzhu2@cs.hku.hk; Ya-Dong Wu and Yan Zhu contribute equally

† giulio@cs.hku.hk

states, whose preparation could not be efficiently verified with previous techniques [1, 34, 35]. After an offline training on simulated data, the trained network is tested with both simulated data and actual experimental data. The results indicate a high success rate in distinguishing pairs of quantum states using incomplete measurement data that are insufficient for a reliable state estimation with maximum likelihood estimation [36] or generative adversarial networks [22]. On the other hand, we observe that state families of larger effective size or larger complexity require a larger amount of data in order for the network to have a satisfactory performance. Our approach can also be used to verify quantum states across different experimental platforms, having access to different types of measurements in each platform. In addition, it can also be used to test for the equivalence of quantum states up to a given set of unitary operations, such as the set of Gaussian unitaries. Finally, this approach can be extended to families of discrete variable systems, such as the family of ground states of the Ising model.

Framework. Two experimenters, Alice and Bob, own two quantum devices producing copies of two unknown quantum states ρ and σ , respectively. Alice and Bob want to determine whether their devices prepare the same quantum state, that is, whether $\rho = \sigma$. To this purpose, they can only perform a limited set of quantum measurements, possibly different for Alice and Bob. In the following, we denote by \mathcal{M}_A (\mathcal{M}_B) the set of measurements accessible to Alice (Bob). Each measurement $\mathbf{M} \in \mathcal{M}_A$ ($\mathbf{M} \in \mathcal{M}_B$) corresponds to a positive operator-valued measure (POVM), that is, a set of positive operators $\mathbf{M} := (M_j)_{j=1}^k$ acting on the system's Hilbert space and satisfying the normalization condition $\sum_{j=1}^k M_j = \mathbb{1}$. To compare their states, Alice and Bob pick two subsets of measurements $\mathcal{S}_A \subset \mathcal{M}_A$ and $\mathcal{S}_B \subset \mathcal{M}_B$, respectively. The measurements can be chosen independently and randomly, but there is no need for Alice and Bob to sample them from the uniform distribution, or from any specific probability distribution. In general, the sets of performed measurements \mathcal{S}_A and \mathcal{S}_B need not be informationally complete.

By performing a measurement $\mathbf{M} \in \mathcal{S}_A$ ($\mathbf{M} \in \mathcal{S}_B$) on multiple copies of ρ (σ), Alice (Bob) obtains a vector of experimental frequencies \mathbf{d} . This classical data is then sent to a verifier, Charlie, whose task is to decide whether ρ and σ are same state. For each measurement $\mathbf{M} \in \mathcal{S}_A$ (\mathcal{S}_B), Alice (Bob) provides Charlie with a pair (\mathbf{m}, \mathbf{d}) , where \mathbf{m} is a parametrization of the measurement \mathbf{M} . Here, the parametrization \mathbf{m} could be either a full description of the POVM \mathbf{M} , or a lower-dimensional parametrization valid only for measurements in \mathcal{M}_A (\mathcal{M}_B).

Here we introduce a deep neural network that determines whether two unknown states are same or not, using limited and noisy data. We call our network StateNet, in analogy to FaceNet [33], a popular neural network for the identification of human faces. StateNet uses a convolutional neural network [37] to produce a low-dimensional

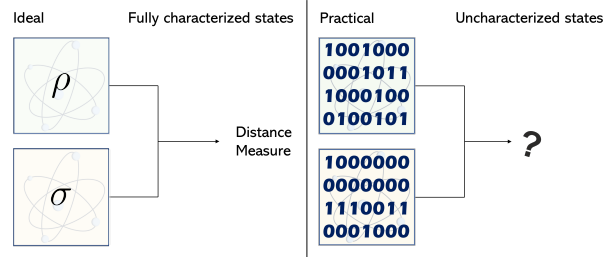


Figure 1. Assessing the similarity of characterized vs uncharacterized quantum states. For fully characterized quantum states (left), the similarity can be assessed by computing their fidelity or any other distance measure. Instead, for uncharacterized quantum states, only measurement data obtained from samples of the states are available (right). The task is then to determine whether two given data sets have been generated from the same state or not. In general, the two data sets can refer to different sets of measurements, and the latter can be noisy and incomplete.

representation of quantum states. For the training, we choose a set of fiducial states and provide the corresponding measurement data to the network. The training data can be generated by computer simulation, or by actual experiments, or by a combination of these two methods. Note that the training data need not be produced afresh; instead, one can use existing data from past simulations or past experiments. For each fiducial state τ , its measurement data set is fed into a deep neural network to produce a low-dimensional representation, given by a vector $\mathbf{r} \in \mathbb{R}^n$. The dimension n is a parameter of the network, and its choice is discussed in the Supplemental Material [38]. Note that in general n can be much smaller than the dimension of the Hilbert spaces containing the fiducial states.

In the training phase, we optimize the parameters of the convolutional neural network with respect to a loss function, called triplet loss [33]. After the training is concluded, the network maps measurement data to vectors that reflect the similarity of quantum states, as illustrated in Supplementary Note 3. Quantum states are then compared by evaluating the Euclidean distance between the corresponding vectors. To decide whether two vectors correspond to the the same quantum state, the network uses a threshold value that balances between the false rejection rate and the false acceptance rate over a new set of unseen measurement data obtained from the fiducial states. The details of StateNet and its training are presented in Supplementary Note 1.

Testing the similarity of continuous variable states. A continuous-variable quantum state ρ is characterized by its Wigner function [39, 40] $W_\rho(\alpha) := \frac{2}{\pi} \text{tr}(\rho D(\alpha)(-1)^{\hat{n}} D(-\alpha))$, where $D(\alpha) := \exp[aa^\dagger - \bar{\alpha}a]$ is a displacement operator, $\hat{n} = \hat{a}^\dagger \hat{a}$ is the photon number operator, and \hat{a}^\dagger and \hat{a} are the bosonic creation operator and annihilation operator respectively. An estimate of the value of $W_\rho(\alpha)$ at any phase-space point α can

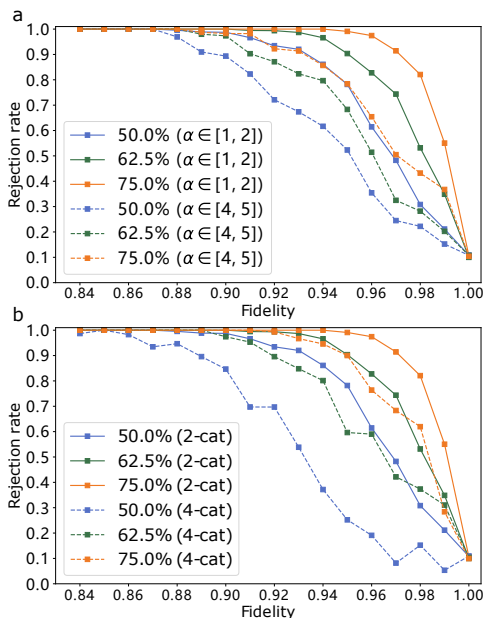


Figure 2. Rejection rate for cat states as a function of the fidelity. Three different scenarios are considered: 50%, 62.5% and 75% of 32×32 pixels are randomly selected as input to the neural network respectively. For all the scenarios, each pixel is an estimate of the Wigner function obtained by sampling the true outcome probability distribution 300 times. In Fig.(a), solid lines are for cat states with $\alpha \in [1, 2]$ and dashed lines are for cat states with $\alpha \in [4, 5]$. In Fig.(b), solid lines are for four-component cat states and dashed lines are for two-component cat states.

be achieved *e.g.* by measuring displaced parity operator $D(\alpha)(-1)^{\hat{n}}D(-\alpha)$, which is widely used for the characterization of quantum states in circuit quantum electrodynamics [41–44].

Suppose that Alice (Bob) can estimate the Wigner function at a finite number of points, chosen at random from a square grid over the phase space. The set of all points on the grid corresponds to the set of achievable measurements $\mathcal{M}_A = \mathcal{M}_B =: \mathcal{M}$. Alice (Bob) randomly chooses a subset of points in the grid to perform measurements of the Wigner function, which is a subset \mathcal{S}_A (\mathcal{S}_B) of \mathcal{M} . In general, the points chosen by Alice and Bob need not be the same. After a finite set of measurement runs, Alice (Bob) obtains a two-dimensional data image, where some pixels are missing and the value at each of the existing pixels is an estimate of the Wigner function at the associated phase-space point. As a result of the finite statistics, the image will generally be blurred.

We test our method on cat states [45, 46] $(|\alpha\rangle + |-\alpha\rangle)/\sqrt{2(1 + \exp(-2|\alpha|^2))}$, where $|\alpha\rangle := D(\alpha)|0\rangle$ is a coherent state. We train StateNet using simulated measurement data from ideal cat states as well as noisy cat states with a fixed amount of thermal noise. After the training is concluded, we test the performance of StateNet in distinguishing between pairs of noisy cat states degraded by photon loss. For each pair of noisy

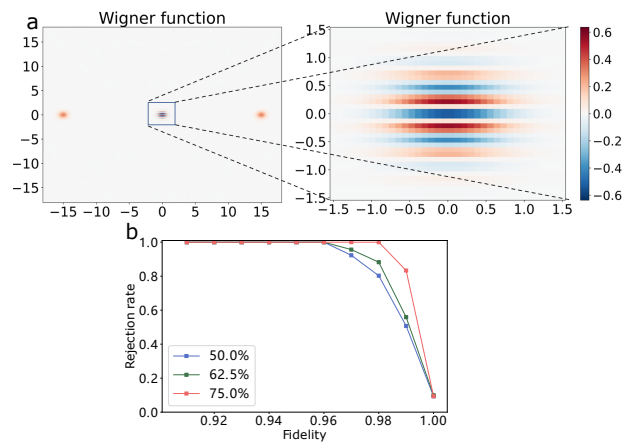


Figure 3. (a) Wigner function of a cat state with $\alpha = 16$, along with a inset figure of the Wigner function on a 36×36 fine grid within the region $[-1.5, 1.5] \times [-1.5, 1.5]$. (b) rejection rates against quantum fidelity when StateNet only utilizes 50%, 62.5%, 75% of the measurement data of the Wigner function on this 36×36 fine grid.

cat states ρ and σ , we take ρ to play the role of the reference state, and make it close to its noiseless counterpart ρ_{ideal} , with fidelity 99%). On the other hand, we regard σ as the untrusted state that needs to be verified, and allow it to be generally noisier, allowing the fidelity with the trusted state ρ to range between 84% and 100%. To evaluate the performance of the network, we plot the rejection rate, namely the probability that the two states are judged to be different, as a function of their fidelity. The resulting plot is shown in Fig. 2.

Fig. 2(a) shows the performance of StateNet for noisy cat states with amplitudes $\alpha \in [1, 2]$ and $\alpha \in [4, 5]$. The numerical results indicate that, when the amplitude is increased without increasing the amount of measurement data, the prediction accuracy decreases. We also test how the performance of our neural network is affected by the states’ complexity, as measured by their nonclassicality [47]. To this purpose, we consider cat-like states that are superposition of four coherent states instead of two. Fig. 2(b) demonstrates that the success rate of StateNet decreases as state complexity increases.

To test the ability of our network to cope with high-dimensional quantum states, we perform numerical experiments on noisy cat states with high amplitudes. Figure 3(b) illustrates the performances of StateNet for the comparison of two noisy cat states with amplitudes $\alpha \in [15, 16]$ (corresponding to an average number of photons between 225 and 256) using displaced parity measurement data on a 36×36 grid within $[-1.5, 1.5] \times [-1.5, 1.5]$ in phase space. Despite the limited amount of measurement data, StateNet achieves a relatively high success rate in this high amplitude scenario.

In addition to cat states, we also consider the family of states of the form

$$|\phi_{\theta, \alpha}\rangle := \text{SNAP}(\theta) |\alpha\rangle, \quad (1)$$

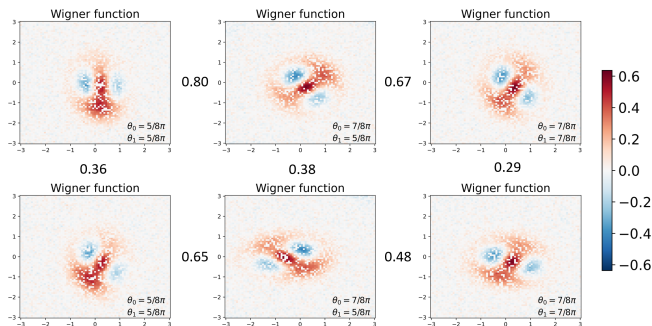


Figure 4. Verification of equivalence up to Gaussian unitary transformations. Each column contains a pair of data images of the same quantum state with different affine transformations. The three different columns correspond to three quantum states (1) with different values of θ_0 and θ_1 ($\theta_n = 0$ for $n \geq 2$). The number between each pair of data images is the Euclidean distance between their state representations produced by StateNet. Each data image contains 4900 pixels randomly chosen from $81 \times 81 = 6561$ pixels, and the value at each pixel is an estimate of the Wigner function obtained by sampling the outcome probability distribution for 500 times.

where $\text{SNAP}(\boldsymbol{\theta}) := \sum_n \exp(i\theta_n) |n\rangle \langle n|$ is a selective number-dependent arbitrary phase gate [43, 48]. In this example, we take $\theta_0 = \theta_1 = \pi$ and $\theta_n = 0$ for every $n \geq 2$. For the training, we used computer simulated measurement data. For the testing, instead, we used actual experimental data obtained from a noisy implementation [22, 42] using a resonator coupled to a superconducting transmon qubit. For the test data sets, we randomly choose 5% of $81 \times 81 = 6561$ experimental data pixels corresponding to the same quantum state (shown in Fig.4(b) in Ref. [22]), and we check whether StateNet correctly attributes two such data sets to same quantum state. The acceptance rate, averaged over multiple trails, is 98%.

Verification of Equivalence up to Gaussian Unitary Operations. A variant of StateNet can be used to decide whether two quantum states are the same up to a unitary transformation in a given set. This functionality can be used to make our comparison method robust to unknown systematic unitary errors taking place on individual quantum devices. A common example of such errors are the errors introduced by poorly calibrated displacement pulses, phase rotations and squeezing [49].

In the Wigner function representation, the combination of displacements, rotations, and squeezing corresponds to an affine transformation in phase space. We use StateNet for testing whether two data images generated from states of the form (1) are equivalent up to an affine transformations. Fig. 4 shows examples of image data for equivalent as well as inequivalent quantum states. By balancing both the false rejection rate and the false acceptance rate, we obtain a distance threshold 0.4, which makes our model accept all pairs of equivalent states, and reject the inequivalent ones. More numerical

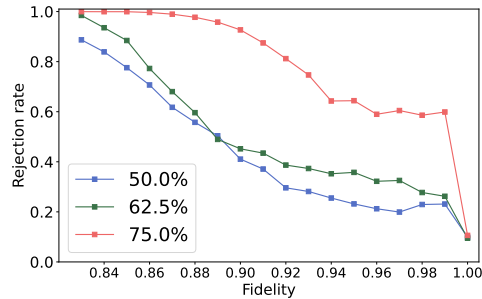


Figure 5. Rejection rate as a function of quantum fidelity for comparing cat states with homodyne measurement data and displaced parity measurement data. For displaced parity measurements, 50%, 62.5% and 75% of 32×32 pixels are randomly selected as input to the neural network respectively, where each pixel is an empirical average of 300 samples. For homodyne measurements, 32 quadrature phases are randomly selected from $[0, \pi)$ and each quadrature phase corresponds to a frequency distribution of 1440 samples.

results are shown in Supplementary Note 4.

Similarity testing with two different sets of achievable measurements. Quantum information protocols have been implemented on a variety of experimental platforms, each involving different sets of feasible measurements. For instance, homodyne measurements are commonly used for photonic systems [36], while displaced parity measurements are preferable in cavity quantum electrodynamics [43, 44]. Here we demonstrate that StateNet test the similarity of quantum states realized on two different experimental platforms, with two different sets of accessible measurements.

We consider a scenario where Alice performs displaced parity measurements on state ρ , while Bob performs homodyne measurements on state σ . Given measurement data from these two essentially different types of measurements, Charlie aims to determine whether ρ equals to σ . To achieve this objective, we jointly train two neural networks, so that their measurement data from these two different types of measurements are mapped into a single representation space. Fig. 5 illustrates the rejection rates against quantum fidelity between two noisy cat states.

Similarity testing for multiqubit states. StateNet can also be adapted to the problem of testing the similarity of multiqubit states, such as the ground states of Ising model. We test its performance on pairs of 10-, 20- or 50-qubit states ρ and σ , where ρ represents an ideal ferromagnetic Ising ground state, and σ an untrusted Ising ground state with poor calibration of the coupling parameters. Alice (Bob) selects a subset of two-qubit nearest-neighbor Pauli measurements, and the measurement statistics is then input into StateNet. The results of our numerical experiments, provided in Supplementary Note 5, show that our approach can correctly identify whether two datasets are from the same ρ or different

states ρ and σ with a probability of over 90% for 10 qubits. However, for 50 qubits, the success probability drops to 80% if the amount of measurement data is kept fixed.

Conclusions. We introduced a model of neural network for testing the similarity of quantum states from limited noisy data. Our work opens up the application of metric learning techniques [50] to the characterization of quantum systems produced by noisy intermediate-scale quantum devices [51]. Furthermore, it sheds light on how machines can discover physical notions, such as the similarity of two quantum states, without any hard-coded information about the corresponding physical theories [52–54].

Acknowledgement. This work was supported by fund-

ing from the Hong Kong Research Grant Council through grants no. 17300918 and no. 17307520, through the Senior Research Fellowship Scheme SRFS2021-7S02, the Croucher Foundation, and by the John Templeton Foundation through grant 62312, The Quantum Information Structure of Spacetime (qiss.fr). YXW acknowledges funding from the National Natural Science Foundation of China through grants no. 61872318. Research at the Perimeter Institute is supported by the Government of Canada through the Department of Innovation, Science and Economic Development Canada and by the Province of Ontario through the Ministry of Research, Innovation and Science. The opinions expressed in this publication are those of the authors and do not necessarily reflect the views of the John Templeton Foundation.

-
- [1] Andreas Elben, Benoît Vermersch, Rick van Bijnen, Christian Kokail, Tiff Brydges, Christine Maier, Manoj K. Joshi, Rainer Blatt, Christian F. Roos, and Peter Zoller, “Cross-platform verification of intermediate scale quantum devices,” *Phys. Rev. Lett.* **124**, 010504 (2020).
- [2] Steven Flammia, “Quantum computer crosscheck,” *Physics* **13**, 3 (2020).
- [3] Jose Carrasco, Andreas Elben, Christian Kokail, Barbara Kraus, and Peter Zoller, “Theoretical and experimental perspectives of quantum verification,” *PRX Quantum* **2**, 010102 (2021).
- [4] Daiwei Zhu, Ze-Pei Cian, Crystal Noel, Andrew Risinger, Debopriyo Biswas, Laird Egan, Yingyue Zhu, Alaina M Green, Cinthia Huerta Alderete, Nhung H Nguyen, *et al.*, “Cross-platform comparison of arbitrary quantum states,” *Nat. Commun.* **13**, 6620 (2022).
- [5] Jens Eisert, Dominik Hangleiter, Nathan Walk, Ingo Roth, Damian Markham, Rhea Parekh, Ulysse Chabaud, and Elham Kashefi, “Quantum certification and benchmarking,” *Nat. Rev. Phys.* **2**, 382–390 (2020).
- [6] Harry Buhman, Richard Cleve, John Watrous, and Ronald de Wolf, “Quantum fingerprinting,” *Phys. Rev. Lett.* **87**, 167902 (2001).
- [7] Lukasz Cincio, Yiğit Subaşı, Andrew T Sornborger, and Patrick J Coles, “Learning the quantum algorithm for state overlap,” *New J. Phys.* **20**, 113022 (2018).
- [8] Ulysse Chabaud, Eleni Diamanti, Damian Markham, Elham Kashefi, and Antoine Joux, “Optimal quantum-programmable projective measurement with linear optics,” *Phys. Rev. A* **98**, 062318 (2018).
- [9] M. Fanizza, M. Rosati, M. Skotiniotis, J. Calsamiglia, and V. Giovannetti, “Beyond the swap test: Optimal estimation of quantum state overlap,” *Phys. Rev. Lett.* **124**, 060503 (2020).
- [10] Leonardo Guerini, Roeland Wiersema, Juan Felipe Carrasquilla, and Leandro Aolita, “Quasiprobabilistic state-overlap estimator for nisq devices,” arXiv preprint arXiv:2112.11618 (2021).
- [11] Anurag Anshu, Zeph Landau, and Yunchao Liu, “Distributed quantum inner product estimation,” in *Proceedings of the 54th Annual ACM SIGACT Symposium on Theory of Computing* (2022) pp. 44–51.
- [12] Carl W Helstrom, “Quantum detection and estimation theory,” *Journal of Statistical Physics* **1**, 231–252 (1969).
- [13] Alexander S Holevo, *Probabilistic and statistical aspects of quantum theory*, Vol. 1 (Springer Science & Business Media, 2011).
- [14] Masahide Sasaki, Alberto Carlini, and Richard Jozsa, “Quantum template matching,” *Phys. Rev. A* **64**, 022317 (2001).
- [15] Vedran Dunjko and Hans J Briegel, “Machine learning & artificial intelligence in the quantum domain: a review of recent progress,” *Reports on Progress in Physics* **81**, 074001 (2018).
- [16] D Zhu, ZP Cian, C Noel, A Risinger, D Biswas, L Egan, Y Zhu, AM Green, C Huerta Alderete, NH Nguyen, *et al.*, “Cross-platform comparison of arbitrary quantum states,” *Nat. Commun.* **13**, 1–6 (2022).
- [17] Giacomo Torlai, Guglielmo Mazzola, Juan Carrasquilla, Matthias Troyer, Roger Melko, and Giuseppe Carleo, “Neural-network quantum state tomography,” *Nat. Phys.* **14**, 447–450 (2018).
- [18] Giacomo Torlai and Roger G. Melko, “Latent space purification via neural density operators,” *Phys. Rev. Lett.* **120**, 240503 (2018).
- [19] Juan Carrasquilla, Giacomo Torlai, Roger G Melko, and Leandro Aolita, “Reconstructing quantum states with generative models,” *Nat. Mach. Intell.* **1**, 155–161 (2019).
- [20] Giacomo Torlai, Brian Timar, Evert P. L. van Nieuwenburg, Harry Levine, Ahmed Omran, Alexander Keesling, Hannes Bernien, Markus Greiner, Vladan Vuletić, Mikhail D. Lukin, Roger G. Melko, and Manuel Endres, “Integrating neural networks with a quantum simulator for state reconstruction,” *Phys. Rev. Lett.* **123**, 230504 (2019).
- [21] Egor S Tiunov, VV Tiunova, Alexander E Ulanov, AI Lvovsky, and Aleksey K Fedorov, “Experimental quantum homodyne tomography via machine learning,” *Optica* **7**, 448–454 (2020).
- [22] Shahnawaz Ahmed, Carlos Sánchez Muñoz, Franco Nori, and Anton Frisk Kockum, “Quantum state tomography with conditional generative adversarial networks,” *Phys. Rev. Lett.* **127**, 140502 (2021).
- [23] Alistair W. R. Smith, Johnnie Gray, and M. S. Kim, “Efficient quantum state sample tomography with basis-

- dependent neural networks,” *PRX Quantum* **2**, 020348 (2021).
- [24] Tobias Schmale, Moritz Reh, and Martin Gärttner, “Efficient quantum state tomography with convolutional neural networks,” *npj Quantum Inf.* **8**, 115 (2022).
- [25] Yan Zhu, Ya-Dong Wu, Ge Bai, Dong-Sheng Wang, Yuexuan Wang, and Giulio Chiribella, “Flexible learning of quantum states with generative query neural networks,” *Nat. Commun.* **13**, 6222 (2022).
- [26] Ekaterina Fedotova, Nikolai Kuznetsov, Egor Tiunov, and AI Lvovsky, “Continuous-variable quantum tomography of high-amplitude states,” *arXiv preprint arXiv:2212.07406* (2022).
- [27] Easwar Magesan, Jay M. Gambetta, A. D. Córcoles, and Jerry M. Chow, “Machine learning for discriminating quantum measurement trajectories and improving readout,” *Phys. Rev. Lett.* **114**, 200501 (2015).
- [28] Juan Carrasquilla and Roger G Melko, “Machine learning phases of matter,” *Nat. Phys.* **13**, 431–434 (2017).
- [29] Jun Gao, Lu-Feng Qiao, Zhi-Qiang Jiao, Yue-Chi Ma, Cheng-Qiu Hu, Ruo-Jing Ren, Ai-Lin Yang, Hao Tang, Man-Hong Yung, and Xian-Min Jin, “Experimental machine learning of quantum states,” *Phys. Rev. Lett.* **120**, 240501 (2018).
- [30] Valeria Cimini, Marco Barbieri, Nicolas Treps, Mattia Walschaers, and Valentina Parigi, “Neural networks for detecting multimode wigner negativity,” *Phys. Rev. Lett.* **125**, 160504 (2020).
- [31] Sebastian J. Wetzel, Roger G. Melko, Joseph Scott, Maysun Panju, and Vijay Ganesh, “Discovering symmetry invariants and conserved quantities by interpreting siamese neural networks,” *Phys. Rev. Research* **2**, 033499 (2020).
- [32] Xiaoqian Zhang, Maolin Luo, Zhaodi Wen, Qin Feng, Shengshi Pang, Weiqi Luo, and Xiaoqi Zhou, “Direct fidelity estimation of quantum states using machine learning,” *Phys. Rev. Lett.* **127**, 130503 (2021).
- [33] Florian Schroff, Dmitry Kalenichenko, and James Philbin, “Facenet: A unified embedding for face recognition and clustering,” in *CVPR* (2015) pp. 815–823.
- [34] Leandro Aolita, Christian Gogolin, Martin Kliesch, and Jens Eisert, “Reliable quantum certification of photonic state preparations,” *Nat. Commun.* **6**, 8498 (2015).
- [35] Ya-Dong Wu, Ge Bai, Giulio Chiribella, and Nana Liu, “Efficient verification of continuous-variable quantum states and devices without assuming identical and independent operations,” *Phys. Rev. Lett.* **126**, 240503 (2021).
- [36] A. I. Lvovsky and M. G. Raymer, “Continuous-variable optical quantum-state tomography,” *Rev. Mod. Phys.* **81**, 299–332 (2009).
- [37] Yann LeCun, Yoshua Bengio, and Geoffrey Hinton, “Deep learning,” *Nature* **521**, 436–444 (2015).
- [38] See Supplemental Material [url] for implementation and training details of our neural network model, which includes Refs. [55–58].
- [39] L. G. Lutterbach and L. Davidovich, “Method for direct measurement of the wigner function in cavity qed and ion traps,” *Phys. Rev. Lett.* **78**, 2547–2550 (1997).
- [40] P. Bertet, A. Auffeves, P. Maioli, S. Osnaghi, T. Meunier, M. Brune, J. M. Raimond, and S. Haroche, “Direct measurement of the wigner function of a one-photon fock state in a cavity,” *Phys. Rev. Lett.* **89**, 200402 (2002).
- [41] Brian Vlastakis, Gerhard Kirchmair, Zaki Leghtas, Simon E Nigg, Luigi Frunzio, Steven M Girvin, Mazhar Mirrahimi, Michel H Devoret, and Robert J Schoelkopf, “Deterministically encoding quantum information using 100-photon schrödinger cat states,” *Science* **342**, 607–610 (2013).
- [42] Marina Kudra, Mikael Kervinen, Ingrid Strandberg, Shah Nawaz Ahmed, Marco Scigliuzzo, Amr Osman, Daniel Pérez Lozano, Mats O. Tholén, Riccardo Borgani, David B. Haviland, Giulia Ferrini, Jonas Bylander, Anton Frisk Kockum, Fernando Quijandria, Per Delsing, and Simone Gasparinetti, “Robust preparation of wigner-negative states with optimized snap-displacement sequences,” *PRX Quantum* **3**, 030301 (2022).
- [43] Reinier W. Heeres, Brian Vlastakis, Eric Holland, Stefan Krastanov, Victor V. Albert, Luigi Frunzio, Liang Jiang, and Robert J. Schoelkopf, “Cavity state manipulation using photon-number selective phase gates,” *Phys. Rev. Lett.* **115**, 137002 (2015).
- [44] V. V. Sivak, A. Eickbusch, H. Liu, B. Royer, I. Tsioutsios, and M. H. Devoret, “Model-free quantum control with reinforcement learning,” *Phys. Rev. X* **12**, 011059 (2022).
- [45] B. Yurke and D. Stoler, “Generating quantum mechanical superpositions of macroscopically distinguishable states via amplitude dispersion,” *Phys. Rev. Lett.* **57**, 13–16 (1986).
- [46] Mazhar Mirrahimi, Zaki Leghtas, Victor V Albert, Steven Touzard, Robert J Schoelkopf, Liang Jiang, and Michel H Devoret, “Dynamically protected cat-qubits: a new paradigm for universal quantum computation,” *New J. Phys.* **16**, 045014 (2014).
- [47] Anatole Kenfack and Karol Życzkowski, “Negativity of the wigner function as an indicator of non-classicality,” *J. Opt. B: Quantum Semiclass.* **6**, 396 (2004).
- [48] Thomas Fösel, Stefan Krastanov, Florian Marquardt, and Liang Jiang, “Efficient cavity control with snap gates,” *arXiv preprint arXiv:2004.14256* (2020).
- [49] Christian Weedbrook, Stefano Pirandola, Raúl García-Patrón, Nicolas J. Cerf, Timothy C. Ralph, Jeffrey H. Shapiro, and Seth Lloyd, “Gaussian quantum information,” *Rev. Mod. Phys.* **84**, 621–669 (2012).
- [50] Matthew Schultz and Thorsten Joachims, “Learning a distance metric from relative comparisons,” *Advances in neural information processing systems* **16** (2003).
- [51] John Preskill, “Quantum computing in the nisq era and beyond,” *Quantum* **2**, 79 (2018).
- [52] Raban Iten, Tony Metger, Henrik Wilming, Lidia del Rio, and Renato Renner, “Discovering physical concepts with neural networks,” *Phys. Rev. Lett.* **124**, 010508 (2020).
- [53] Daniel Flam-Shepherd, Tony C Wu, Xuemei Gu, Alba Cervera-Lierta, Mario Krenn, and Alan Aspuru-Guzik, “Learning interpretable representations of entanglement in quantum optics experiments using deep generative models,” *Nat. Mach. Intell.* **4**, 544–554 (2022).
- [54] Mario Krenn, Robert Pollice, Si Yue Guo, Matteo Aldeghi, Alba Cervera-Lierta, Pascal Friederich, Gabriel dos Passos Gomes, Florian Häse, Adrian Jinich, Akshat Kumar Nigam, *et al.*, “On scientific understanding with artificial intelligence,” *Nat. Rev. Phys.* , 1–9 (2022).
- [55] Charu C Aggarwal *et al.*, “Neural networks and deep learning,” *Springer* **10**, 978–3 (2018).
- [56] J Robert Johansson, Paul D Nation, and Franco Nori, “Qutip: An open-source python framework for the dynamics of open quantum systems,” *Computer Physics Communications* **183**, 1760–1772 (2012).

[57] Francois Chollet *et al.*, “Keras,” (2015).

[58] Laurens Van der Maaten and Geoffrey Hinton, “Visualizing data using t-sne.” *J. Mach. Learn. Res.* **9** (2008).

SUPPLEMENTARY INFORMATION

Supplementary Note 1 Implementation details of StateNet

A. Structure of StateNet

As shown in Supplementary Fig. 6, our proposed StateNet for learning quantum state similarity consists of a representation network f_{ξ} and a L_2 normalization layer.

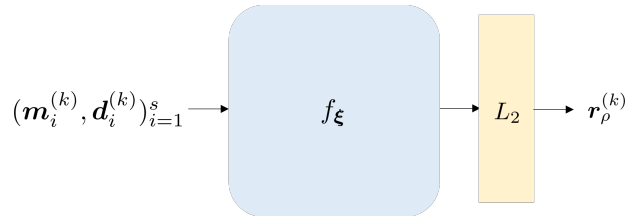


Figure 6. Structure of StateNet.

The representation network f_{ξ} is composed of multiple convolutional layers, a max pooling layer, a dropout layer and a last full-connected layer [55] and we depict its structure in Supplementary Fig. 7. We denote all trainable parameters in the representation network as ξ . The input of the representation network is a set of s measurement results of a quantum state and we denote them as $(\mathbf{m}_j^{(k)}, \mathbf{d}_j^{(k)})_{j=1}^s$, where \mathbf{m}_j is parameterization of the measurement and \mathbf{d}_j is a vector of experimental measurement outcome frequencies on the state. A L_2 normalization layer following the representation network is used for rescaling the output of the representation network to have Euclidean norm 1.

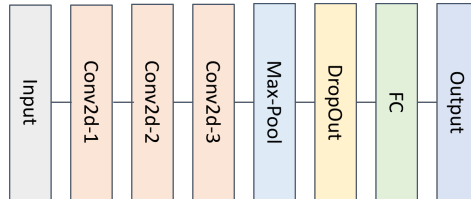


Figure 7. Structure of the representation network.

B. Training Details

a. Loss function. In the training, we adopt a loss function called Triplet Loss used in FaceNet. The Triplet Loss minimizes the distance between an anchor and a positive, both of which belong to the same quantum state, and maximizes the distance between the anchor and a negative which belongs to different quantum states. In each round of optimization, we choose a representation $\mathbf{r}_{\tau}^{(l)}$ as a reference with a fixed state τ and l . Then, we compare the Euclidean distances $\|\mathbf{r}_{\tau}^{(l)} - \mathbf{r}_{\tau}^{(i)}\|_2$ of state representations associated to different measurements on the same state τ , with the Euclidean distances $\|\mathbf{r}_{\tau}^{(l)} - \mathbf{r}_{\xi}^{(m)}\|_2$ of state representations associated to different states τ and ξ , for every $1 \leq i \leq K$, $i \neq l$, $1 \leq m \leq K$, and for a randomly chosen fiducial state $\xi \neq \tau$. Optimizing triplet loss aims to minimize $\|\mathbf{r}_{\tau}^{(l)} - \mathbf{r}_{\tau}^{(i)}\|_2$ for multiple rounds of experiments with respect to same fiducial state τ , and simultaneously maximize $\|\mathbf{r}_{\tau}^{(l)} - \mathbf{r}_{\xi}^{(m)}\|_2$ for each pair of different fiducial states $\tau \neq \xi$. The detailed steps of training is presented in Algorithm 1.

Algorithm 1: Training of StateNet for learning quantum state similarity.

Data: number of states in training set N , state measurement results $\{\{\chi_{\rho_i}^{(k)}\}_{k=1}^K\}_{i=1}^N$, maximum number of epochs E , learning rate δ

Initialize parameters ξ and randomly, $e = 0$;

while $e < E$ **do**

 Calculate the state representation $r_{\rho_i}^{(k)}$ for each state measurement result $\chi_{\rho_i}^{(k)}$;

$\mathcal{L} = 0$;

for $i_1 = 1$ **to** N **do**

 Randomly select K state representations $r_{\rho_j}^{(k)}$ from all state representations, where $j \neq i_1$, and denote them as

$\{r_{\rho_{neg}}^{(k)}\}_{k=1}^K$;

for $i_2 = 1$ **to** K **do**

 Select $r_{\rho_{i_1}}^{(i_2)}$ as a reference state representation;

 Calculate the Euclidean distance $\text{dist}_k := \|r_{\rho_{i_1}}^{(i_2)} - r_{\rho_{i_1}}^{(k)}\|_2$ between $r_{\rho_{i_1}}^{(i_2)}$ and each $r_{\rho_{i_1}}^{(k)}$, where

$k \in \{1, 2, \dots, K\}$;

 Calculate the Euclidean distance $\|r_{\rho_{i_1}}^{(i_2)} - r_{\rho_{neg}}^{(k)}\|_2$ between $r_{\rho_{i_1}}^{(i_2)}$ and each element in $\{r_{\rho_{neg}}^{(k)}\}_{k=1}^K$ and find the minimum $\text{dist}_{neg} := \min_k \|r_{\rho_{i_1}}^{(i_2)} - r_{\rho_{neg}}^{(k)}\|_2$;

$\mathcal{L} = \mathcal{L} + \sum_{k=1}^K \text{dist}_k - K \cdot \text{dist}_{neg}$;

 Update ξ as $\xi = \xi - \delta \nabla_{\xi} \mathcal{L}$;

$e = e + 1$;

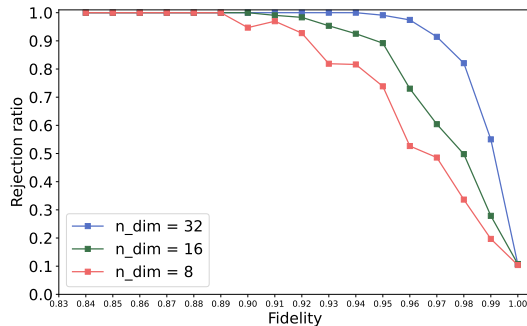


Figure 8. The rejection rates as functions of quantum fidelity between two noisy cat states with respect to different state representation dimensions $n = 32, 16$ and 8 .

b. Training set and validation set. Both the training and the validation sets are simulation data in our experiments. We usually generate all of the simulated data and apportion the data into training and validation sets, with an 80-20 split. The model is first trained over the training set and the threshold is then chosen over the validation set by minimizing both the false rejection rate and the false acceptance rate.

c. Initialization and learning rate. We randomly initialize the parameters of the StateNet in each experiment and set the initial learning rate as 0.01. We decrease the learning rate as the number of iterations increases.

d. Number of epochs and training time. The maximum number of epochs E is usually set as 500 in the training. The training time depends on the specific dataset and tasks we consider but it is less than one hour in all of the experiments shown in this paper.

e. Dimension of state representations. The dimension of the state representation space is set to be $n = 32$ for all the numerical experiments. Changing the dimension of state representations affects the performance of our data-driven approach. When we reduce the dimension of state representations from 32 to 8, we find clear reduction of success rates in distinguishing two noisy states only when quantum fidelity is above 0.9 and below one, as shown in Fig. 8.

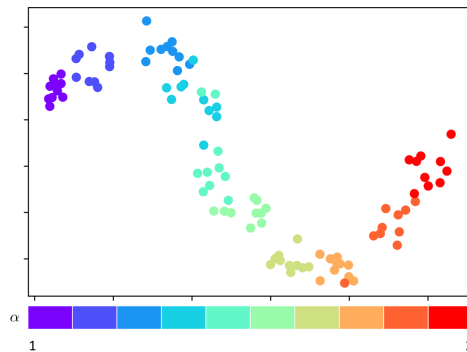


Figure 9. 2D projections of state representations corresponding to cat states $\propto |\alpha\rangle + |-\alpha\rangle$ with $\alpha \in \{1, 1.1, \dots, 1.9\}$ obtained by t-SNE. In the figure, points of the same color correspond to state representations associated to different measurements on the same quantum state.

Supplementary Note 2 Dataset

In this section, we will introduce the types and the generation method of the fiducial states used in the settings we consider.

a. Cross-Platform Verification of Quantum States The training set is composed of the simulated measurement data of both ideal cat states in Eq. (1) with $\alpha \in \{1, 1.1, \dots, 2\}$ and noisy cat states with certain amount of thermal noises. The test set is composed of noisy cat states with photon loss errors. In order to test our model for noisy experimental data, we also use simulated measurement data of states in Eq. (2) with $\alpha \in \{\frac{\pi}{2}, \frac{5\pi}{8}, \dots, \frac{3\pi}{2}\}$ to train our proposed model. All of these states are generated by qutip [56].

b. Cross-Platform Verification of Quantum Dynamics In this experiment, fiducial states in the training set is composed of all the states at different time step t_i when the states are initialized in coherent states with $\alpha \in \{1, 1.1, \dots, 2\}$. All of these states are generated by qutip [56]. The test set consists of quantum states under the noiseless quantum evolution and the noisy quantum evolution.

c. Cross-Platform Verification of Equivalence up to Unitary Operations In this setting, our proposed StateNet is trained by the measurement data corresponding to the states in Eq. (2) with $\theta_0, \theta_1 \in \{\pi/2, 3\pi/4, \dots, 3\pi/2\}$ and tested by the measurement data corresponding to the states with $\theta_0, \theta_1 \in \{5\pi/8, 7\pi/8, \dots, 11\pi/8\}$. The states are generated by qutip [56] and the affine transformations are simulated by tools provided in Keras [57].

Supplementary Note 3 Visualization of State Representations

It is also useful to visualize the state representations obtained by embedding different measurement data in feature space. To this purpose, we feed the state representations of training states with $\alpha \in \{1, 1.1, \dots, 1.9\}$, into a t-distributed stochastic neighbor embedding (t-SNE) algorithm [58] to project the representation vectors into a two-dimensional plane, according to their similarities in feature space. The results, provided in Fig. 9, show that measurement data associated to the same state effectively correspond to nearby vectors, while measurement data associated to different states typically correspond to distant vectors. It is worth stressing that StateNet was not provided with any state parameter (*e.g.* it was not provided the value of α), nor it was provided any information about the fidelity of quantum states. The notion of distance visualized in the figure was developed by the network as a way to minimize the loss function in the training phase.

Supplementary Note 4 Verification of Equivalence up to Gaussian Unitary Operations

In the Wigner function representation, the combination of displacements, rotations, and squeezing corresponds to the following affine transformation in phase space

$$\begin{pmatrix} x \\ p \end{pmatrix} \rightarrow \begin{pmatrix} \zeta(x \cos \phi + x \sin \phi + \Delta_x) \\ 1/\zeta(p \sin \phi + p \cos \phi + \Delta_p) \end{pmatrix},$$

where ϕ is a rotation angle, Δ_x and Δ_p are shifts in position and momentum, respectively, and ζ is a squeezing parameter. Each data image, with respect to quantum states (1) in main text with $\theta_0, \theta_1 \in [\pi/2, 3\pi/2]$ and $\theta_n = 0$ for $n \geq 2$, undergoes an affine transformation with uniformly random parameters $\phi \in [0, \pi)$, $\Delta_x, \Delta_p \in (-1, 1)$ and $\zeta \in [5/6, 6/5]$. Then data images with same values of θ but different affine transformations are labeled the same, while data images with different values of θ are identified with different labels.

We train StateNet with data corresponding to $\theta_0, \theta_1 \in \{\pi/2, 3\pi/4, \dots, 3\pi/2\}$ and then test it over unseen data images corresponding to $\theta_0, \theta_1 \in \{5\pi/8, 7\pi/8, \dots, 11\pi/8\}$ to decide whether two data images correspond to the same quantum state up to certain distortion effect. Numerical results show that both the average rate to reject different labels and the average rate to accept same labels is around 90%.

Supplementary Note 5 Verification of Ising ground states

In this section, we apply our method to verification of many-qubit states. We consider 10-, 20- and 50-qubit ground states of ferromagnetic Ising model. The Hamiltonian of Ising model is

$$H = - \left(\sum_{i=0}^{L-2} J_i \sigma_i^z \sigma_{i+1}^z + \sum_{j=0}^{L-1} \sigma_j^x \right), \quad (2)$$

where coupling parameters $J_i > 0$ correspond to ferromagnetic interactions. Here the measurement set \mathcal{M} consists of all two-qubit Pauli measurements on nearest-neighbor qubits. Alice (Bob) can randomly choose a subset of measurements from \mathcal{M} and we denote it as $\mathcal{S}_A(\mathcal{S}_B)$. Note that \mathcal{S}_A can be different from \mathcal{S}_B . After a finite set of measurement runs, Alice (Bob) will collect $|\mathcal{S}_A|(|\mathcal{S}_B|)$ measurement outcome probability distributions corresponding to $\mathcal{S}_A(\mathcal{S}_B)$.

We train StateNet using simulated measurement data from ideal ground states of the Ising model in Eq. (2). After the training is concluded, we test the performance of StateNet in the cross-verification of pairs of states ρ and σ . For each pair, we randomly choose $J \in [0.3, 0.4)$ and make ρ an ideal Ising ground state with $J_i = J$, which plays the role of the reference state. On the other hand, we regard σ as the untrusted state that needs to be verified, and make it degraded by poor calibration of coupling parameters, where J_i becomes a Gaussian random variable with mean value J and variance 0.1. In Supplementary Table I, we show the acceptance rates for the same ideal ground states and the rejection rates for different states in the test.

Acceptance/rejection rates	10-qubit	20-qubit	50-qubit
50% of measurement data	0.96/0.93	0.91/0.87	0.84/0.80
62.5% of measurement data	1/1	0.95/0.93	0.89/0.89
75% of measurement data	1/1	0.96/0.93	0.92/0.90

Table I. The acceptance rates for same state and the rejection rates for different states with respect to 10-, 20-, and 50-qubit ground states of Ising model when \mathcal{S}_A and \mathcal{S}_B consist of 50%, 62.5% and 75% of \mathcal{M} .